ISSN (Print) 1226-1750
ISSN (Online) 2233-6656
Journal of Magnetics 28(3), 317-322 (2023) https://doi.org/10.4283/JMAG.2023.28.3.317

Reinforcement of the Magnetic Lens Effect in the Dipole Magnet for a Neutral Beam Injector

Geonwoo Baek, Jinhyun Jeong, Min Park, Byungkeun Na, Seul Chan Hong, and Jong-Gu Kwak*

High Temperature Plasma Research Division, Korea Institute of Fusion Energy, Daejeon 34133, Republic of Korea

(Received 16 January 2023, Received in final form 14 July 2023, Accepted 18 July 2023)

Dipole magnet for a neutral beam injector is a magnetic device deflecting residual ions to an ion dump. For the high power neutral beam injection to fusion plasma, the heat load on the surface of the residual ion dump should be under acceptable level. We investigate the magnetic lens effect of the bending magnet for beam expansion cases. To intensify the magnetic lens effect, the height of the field clamp in the magnetic core is adjusted. The COMSOL Multiphysics software is employed to calculate a magnetic flux density for the dipole magnet, to trace an ion beam trajectory, and to evaluate a heat distribution on the beam dump. Simulation results reveal that the longitudinal magnetic field at the magnet entrance has a significant effect on the heat distribution in the ion dump surface, and hence the local heat flux is considerably alleviated by the field clamp with adjusting the height of the clamp.

Keywords : dipole magnet, field clamp, magnetic lens, neutral beam injection

1. Introduction

The neutral beam injection (NBI) has been proved to be powerful means for the plasma heating and current drive in tokamak devices, such as the DIII-D, JET, JT-60U, and KSTAR [1-4]. Accordingly, two NBI injectors, each delivering 16.7 MW beam power, were planned to be installed in the ITER fusion reactor to be the largest fusion experiment in the world [5]. The KSTAR has been equipped with two NBI injectors, named as NB-1 and NB-2 [6]. In the 2022 KSTAR campaign, the NB-1 and NB-2 provided heating powers of 3.6 MW and 4.0 MW, respectively. Until 2025, the NB-2 should deliver the neutral beam with the heating power of 6 MW into the tokamak plasma. To achieve such target of the NBI beam power, the power deposition on beamline components should be acceptable [7]. Among beamline components, an ion dump and a calorimeter usually receive the strongest heat flux.

There were various efforts to reduce the power density on the ion beam dump. Raster scanning method with the phase modulation of the magnet current was proposed to relieve the time-averaged heat flux by W. K. Dagenhart *et al.* [8]. K. Sakurai *et al.* investigated the effect of the fringe field on the power deposition profile of the ion dump surface in a 180° bending magnet system [9]. The bending magnet of the KSTAR NBI injector was designed by S.R. In *et al.*, and they explained the vertical expansion of the ion beam on the dump by a magnetic lens effect [10]. However, the bending magnet was not optimized with respect to the magnetic lens effect because of limitations in computer performance at that time. Further reinforcement of the magnetic lens effect can be possible by modifying topology of a magnetic core, which is composed of poles, yokes, and field clamps, to alleviate the maximum heat load on the ion dump surface.

In this paper, the field clamp of the magnetic core is chosen to intensify the magnetic lens effect based on two important considerations: (1) sensitivity of end fields and (2) cost efficiency related with fabrication. While adjusting the height of the field clamp in existing NB-2 dipole magnet, magnetic characteristics, beam trajectories, and heat loads are numerically calculated with the COMSOL Multiphysics software [11]. In section 2, the KSTAR NB-2 bending magnet is modeled to investigate the magnetic characteristic of it. The magnetic field obtained is set as input data for the ion beam simulation. The ion beam released from an ion source is traced in section 3. The heat flux is also estimated on the beam dump surface.

*Corresponding author: Tel: +82-42-879-5113
e-mail: jgkwak@kfe.re.kr

Section 4 includes conclusions and future work.

2. Magnetic Characteristic of NB-2 Dipole Magnet

2.1. Dipole Magnet Modeling

An NBI system is usually consists of an ion source, a neutralizer, a dipole magnet, an ion dump, a calorimeter, and a beam duct [12]. The KSTAR NB-2 has been equipped with three ion sources and three beamlines [6]. Three magnets in all the beamlines are identically fabricated, and there is no interference with each other during the magnet operation. Hence, it is sufficient to model only one bending magnet to analyze the magnetic characteristic and track ion beam trajectories. This assumption can significantly relieve the computational load.

Fig. 1 depicts the 2D cross-sectional view (all dimensions are in mm), and 3D full geometry of the bending magnet installed in the NB-2. The bending magnet is made up of two racetrack coils wound with an oxygen-free high conductivity copper, poles, yokes, and field clamps. The number of turns is 48 in each racetrack coil. The magnetic core was assembled using a bolted joint. The magnetic material of a low carbon steel (i.e., SAE 1006) was used due to its high permeability, low remanence, and narrow hysteresis loop.

The magnetic flux density can be calculated using the A-formulation:

$$\vec{\nabla} \times \vec{A} = \vec{B} \tag{1}$$

$$\vec{B} = \mu_0 \mu_r \vec{H} \tag{2}$$

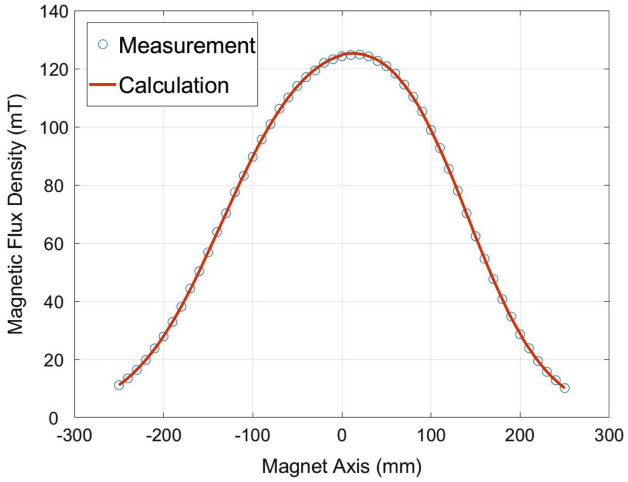

Fig. 2. (Color online) Comparison of calculated values of the vertical magnetic field with measured ones along the beam axis. The magnet center is at 0 mm. The circles and solid line represent measured and calculated magnetic flux densities, respectively.

$$\vec{\nabla} \times \vec{H} = \vec{J} \tag{3}$$

where **A** is the magnetic vector potential, **B** is the magnetic flux density, **H** is the magnetic field intensity, μ_0 is the permeability of the vacuum, μ_r is the relative permeability of the material, and **J** is the current density. The components of the magnetic vector potential are state variables.

The model of the NB-2 dipole magnet can be validated by comparing calculated values of the vertical magnetic field, which is perpendicular to the beam axis, with measured ones. The excitation current of the magnet is set to 300 A. Fig. 2 shows the calculated magnetic field is

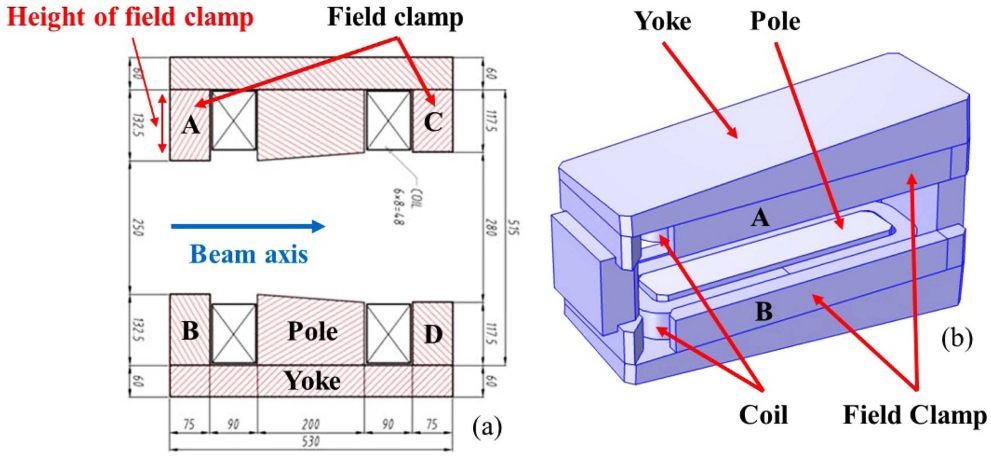

Fig. 1. (Color online) The schematic diagram of the KSTAR NB-2 bending magnet: (a) 2D cross-sectional view (all dimensions are in mm) and (b) 3D full geometry.

almost equal to the measured one. Quantitatively, the relative errors are less than 1.50 %. Therefore, the modeling of the bending magnet using the COMSOL Multiphysics can be said to be successful.

2.2. Field Analysis of Dipole Magnet

In an accelerator magnet, the longitudinal field component to the beam axis has a negligible effect on the charged particle motion [13]. However, in an NBI magnet, the longitudinal field component plays an important role because the bending magnet is intentionally tilted about the beam axis to produce the solenoid lens effect. Since the KSTAR NB-2 bending magnet is tilted by 45° to the beam direction, residual ions have transverse and longitudinal velocity components at the magnet entrance. The ion beam entering the bending magnet is focused by the transverse velocity component and longitudinal magnetic field. Passing through focal points, the ion beam is vertically expanded towards the ion dump. Because the projection area of the ion beam on the ion dump is closely related to the maximum heat flux, it can be mitigated by the vertical beam expansion.

Fig. 3 shows the vertical and longitudinal magnetic flux densities at the reference radius, commonly about two-thirds of a beam aperture [13, 14], along the straight beam axis in the NB-2 bending magnet. They are calculated at a certain point on the reference radius, having the highest value of the magnetic field. The maximum vertical and longitudinal fields are 149.1 mT and 86.6 mT, respectively, and hence the longitudinal field might have a considerable effect on the ion beam trajectory in the 45° tilted bending magnet. The Lorentz force acting upon the particle with the energy of 70 keV is approximately calculated as 2.54×10^{-14} N at the magnet entrance.

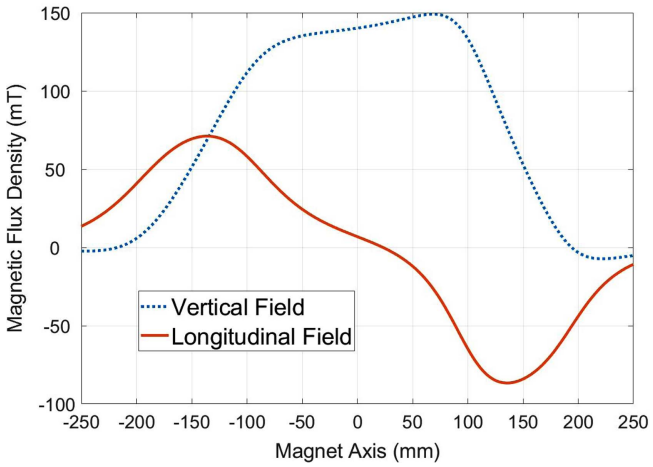

Fig. 3. (Color online) The vertical and longitudinal magnetic fields at a certain point on the reference radius along the beam axis. The operation current of the magnet is set to 300 A. The dotted and solid lines represent the vertical and longitudinal fields, respectively.

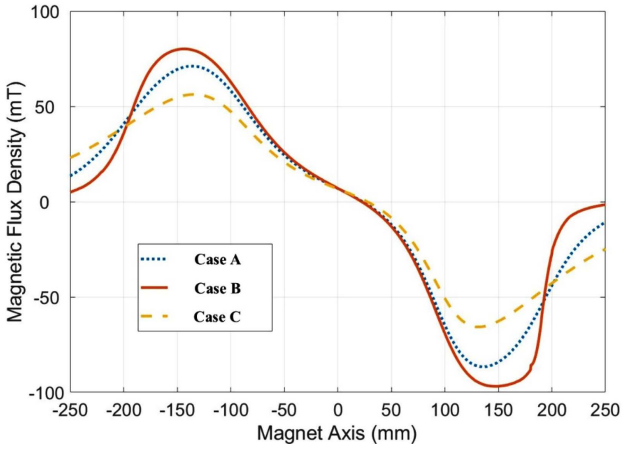

Fig. 4. (Color online) Variation of longitudinal fields generated by bending magnets with different heights of the field clamp. The magnetic field is calculated at a certain point on the reference radius along the beam axis. The magnet current is set to 300 A. The dotted, solid, and dashed lines represent Cases A, B, and C, respectively.

We resize the height of the field clamp in the magnetic core to adjust the longitudinal magnetic field at the magnet entrance. The field clamp seems to be an appropriate selection considering the influence on end fields and the cost efficiency. In practice, the field clamp plays the role of suppressing the fringe field at coil ends by the flux shunting [15]. If there is no field clamp in the dipole magnet, the fringe field becomes stronger, so that the longitudinal magnetic field related with the magnetic lens effect decreases.

Longitudinal fields generated by three cases of magnets are compared as shown in Fig. 4. Case A considers the already fabricated and installed NB-2 bending magnet in which heights of four field clamps are indicated in the 2D drawing of Fig. 1. Heights of four field clamps are extended by 32.5 mm for Case B. In Case C, there is no field clamp in the magnet, i.e., heights of four field clamps are set to 0 mm. As expected, the field clamp with the higher height brings about the stronger longitudinal magnetic field, and hence it is expected to intensify the solenoid lens effect of the bending magnet.

3. Simulation of Ion Beam Trajectory

3.1. Particle Release Modeling

An ion source is usually composed of a plasma generator and an accelerator. In the KSTAR NB-2, deuterium

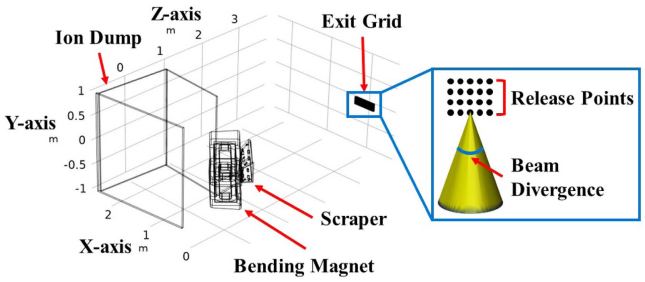

Fig. 5. (Color online) Solution region including the ground grid, bending magnet with scraper, and ion dump. The deuterium ion beam propagates from the exit grid towards the bending magnet. There is an enlarged view of the exit grid portraying the particle release.

ions from an arc chamber are accelerated by multi-aperture accelerating grids, which are made up of plasma, gradient, suppressor, and ground grids [16]. After the deuterium ion beam leaves the ground grid, residual ions from the neutralizer are dumped to the beam dump by interacting with the magnetic field of the bending magnet. Fig. 5 presents the solution region including the exit grid, bending magnet with scraper, and ion dump. There are 280 apertures in the ground grid, and the distance between the exit grid and bending magnet is 3,800 mm.

For the particle release modeling, it is assumed that: (1) 100 particles are released at the center of each aperture in the exit grid, so a total number of released particles is 28,000, (2) particles at each aperture are released in a conical shape in which apex angle is equivalent to a beam divergence, (3) the particle species is positively charged atomic deuterium (D^+), and (4) the particle energy is set as 70 keV. Fig. 5 shows an enlarged view of the ground grid for describing the particle release. The beam divergence is 1° in the KSTAR NB-2 [16].

Newton's second law for motion of charged particle only under the magnetic field can be expressed as follows:

$$\frac{d^2\vec{r}}{dt^2} = \frac{q}{m}(\vec{v} \times \vec{B}) \tag{4}$$

where **r** is the displacement vector, q is the electric charge, m is the mass, **v** is the velocity vector of the particle, and **B** is the magnetic field vector. For simplicity, Coulomb interaction between charged particles is neglected. The second-order ordinary differential equation can be numerically solved by the generalized-alpha method [17].

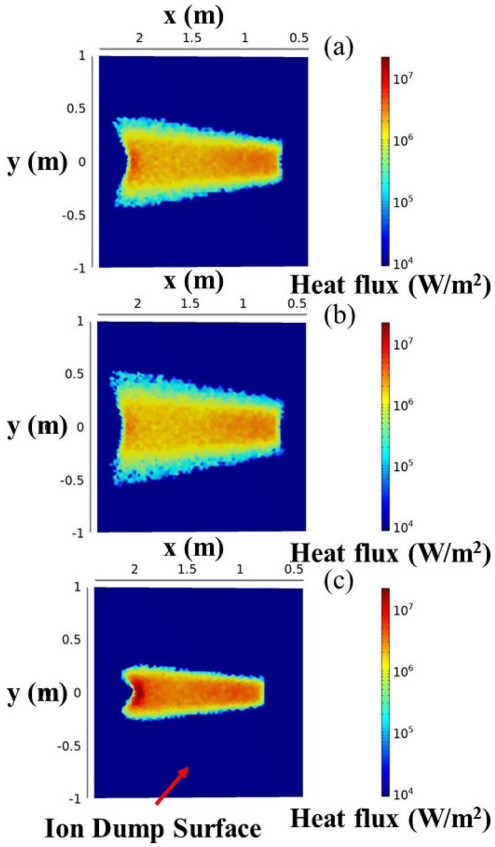

Fig. 7. (Color online) Heat flux distribution on the ion dump surface of (a) Cases A, (b) B, and (c) C.

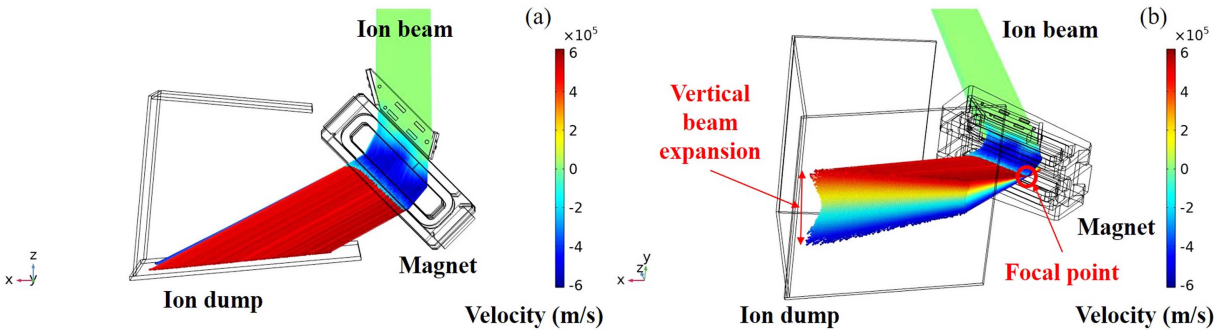

Fig. 6. (Color online) Simulation of the ion beam trajectory of Case A in the solution region. The legend indicates the vertical velocity component of the ion beam: (a) top view and (b) diagonal view.

3.2. Ion Beam Trajectory and Heat Load

Fig. 6 depicts the ion beam trajectory affected by the magnetic field distribution of Case A. The ion beam is deflected to the ion dump, and the vertical velocity component of the ion beam increases while the ion beam passes the dipole magnet. It is noted that the ion beam is vertically expanded on the ion beam dump by the vertical velocity component of the ion beam. To investigate the effect of the field clamp on the heat load, beam trajectories of Cases B and C are simulated. Since both vertical and longitudinal magnetic fields depend on the shape of the field clamp, vertical field integrals of Cases A, B, and C are fixed to 5,300.5 mT·cm by controlling the magnet current to exclude the additional deflection.

Fig. 7 shows the heat flux distribution on the ion dump surface of Cases A, B, and C. The effect of the field clamp on the projection area is obvious. The maximum heat loads of Cases A, B, and C are 6.87 MW/m^2, 4.36 MW/m^2, and 21.3 MW/m^2, respectively. It is noted that the field clamp with the higher height of the dipole magnet results in more vertical beam expansion, thereby less local heat flux. The maximum heat flux of Case B is reduced by about 36.5 % compared with Case A (i.e., already fabricated and installed NB-2 magnet).

Fig. 8 illustrates the vertical component of the Lorentz force, which leads to the focusing of the ion beam, for Cases A, B, and C. It can be seen that the vertical force component exists only in the magnet entrance for all three cases. The vertical force of Case A is similar to the expected value, 2.54×10^{-14} N. The simulation results suggest that the field clamp with the higher height brings about more vertical Lorentz force, e.g., 5.00×10^{-14} N for Case B. It is trivial that more vertical force component induces more vertical beam expansion, thereby weaker heat spot on the ion dump surface.

We also visualize focal lines of Cases A, B, and C as shown in Fig. 9 to clearly show the effect of the field clamp on the focal length of the magnetic lens. To visualize focal lines on ion beam trajectories, vertical

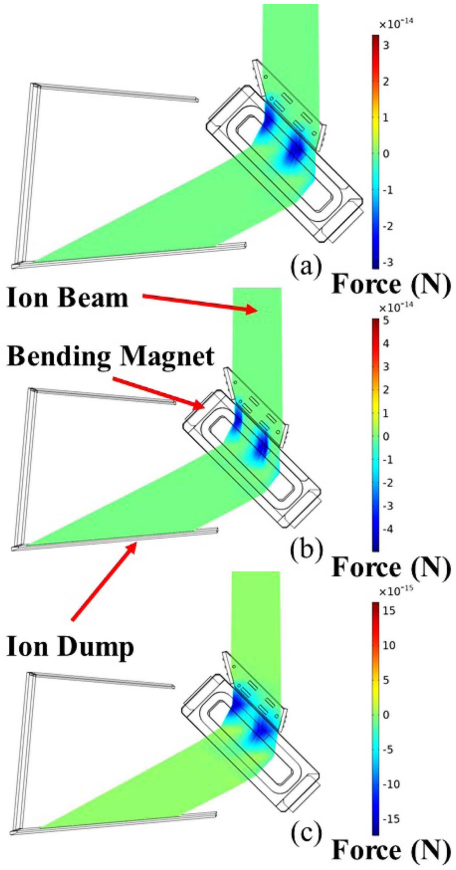

Fig. 8. (Color online) Distribution of the vertical magnetic force acting on charged particles for (a) Cases A, (b) B, and (c) C.

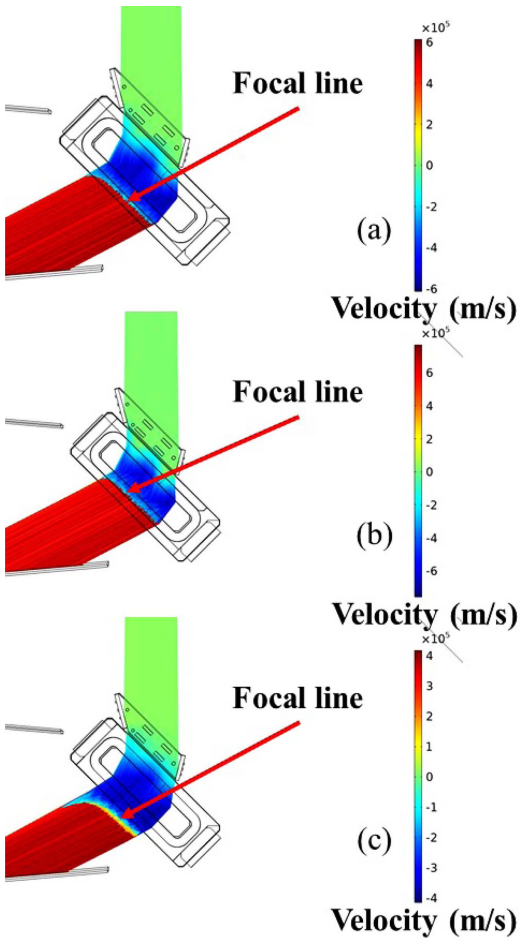

Fig. 9. (Color online) Distribution of the vertical velocity component for (a) Cases A, (b) B, and (c) C. Red arrows indicate focal lines on ion beam trajectories: (a) Case A, (b) B, and (c) C.

velocity components of charged particles are calculated, and then lines at which positive and negative values intersect are defined as focal lines. It is definitely observed that the field clamp with the higher height causes the focal line closer to the magnet entrance.

In summary, to avoid the heat spot at a certain position on the ion dump for the KSTAR NB-2 injector, the height of the field clamp in the magnetic core is adjusted to intensify the magnetic lens effect of the dipole magnet. Through the ion beam trajectory simulation with the COMSOL Multiphysics software, it can be seen that the field clamp with the higher height results in less local heat flux on the dump surface.

4. Conclusion

The reduction in the maximum heat load on the residual ion dump is one of key issues to resolve for 6 MW neutral beam power of the KSTAR NB-2. We are interested in the magnetic lens effect of the dipole magnet in which purpose is to deflect residual ions to the dump. By adjusting the height of the field clamp in the magnetic core, the solenoid lens effect is enhanced, thereby the ion beam is more vertically expanded. By extending heights of original field clamps by 32.5 mm, the maximum heat load on the ion dump surface is alleviated by about 36.5 % compared with the original NB-2 bending magnet. In future work, it is necessary to find more improving shape for the magnetic core of the dipole magnet with a topology optimization algorithm to further relieve the maximum heat load on the residual ion dump.

Acknowledgements

This research was supported by the R&D Program of “KSTAR Experimental Collaboration and Fusion Plasma Research (EN2301-14)” through the Korea Institute of Fusion Energy (KFE) funded by the Government funds.

References

[1] J. T. Scoville, M. D. Boyer, B. J. Crowley, N. W. Eidietis, C. J. Pawley, and J. M. Rauch, Fusion Eng. Des. **146**, 6 (2019).
[2] T. T. C. Jones, *et al.*, Fusion Eng. Des. **47**, 205 (1999).
[3] M. Kuriyama, *et al.*, Fusion Eng. Des. **39-40**, 115 (1998).
[4] Y. S. Bae, *et al.*, Fusion Eng. Des. **87**, 1597 (2012).
[5] R. S. Hemsworth, *et al.*, New J. Phys. **19**, 025005 (2017).
[6] J. H. Jeong, H. S. Ahn, W. Cho, and Y. S. Kim, Fusion Eng. Des. **169**, 112479 (2021).
[7] T. S. Kim, *et al.*, Rev. Sci. Instrum. **87**, 02B317 (2015).
[8] W. K. Dagenhart and T. C. Tucker, J. Appl. Phys. **56**, 22 (1984).
[9] K. Sakurai, Y. Oka, O. Kaneko, and T. Kuroda, Rev. Sci. Instrum. **59**, 2163 (1988).
[10] S. R. In, B. J. Yoon, and B. Y. Kim, Nucl. Eng. Technol. **38**, 793 (2006).
[11] 2023. [Online]. Available: https://www.comsol.com/
[12] H. S. Staten, IEEE Trans. Nucl. Sci. **26**, 1266 (1979).
[13] S. Russenschuck, Field Computation for Accelerator Magnets, Wiley, 2010.
[14] K. H. Mess, S. Wolff, and P. Schmüser, Superconducting Accelerator Magnets, World Scientific, 1996.
[15] H. Hübner and H. Wollnik, Nucl. Instr. and Meth. **86**, 141 (1970).
[16] T. S. Kim, S. H. Jeong, and S. R. In, Rev. Sci. Instrum. **83**, 02B112 (2012).
[17] J. Chung and G. M. Hulbert, J. Appl. Mech. **60**, 371 (1993).